Tellus (1990), *42A*, 92–108

A model-based diagnostic study of the development and maintenance mechanism of two polar lows

By THOR ERIK NORDENG, *The Norwegian Meteorological Institute, P.O. Box 43, Blindern, N-0313 Oslo 3, Norway*

(Manuscript received 9 January 1989; in final form 8 May 1989)

ABSTRACT

The life cycles of two polar lows in the Norwegian Sea have been studied. Both lows were observed, analysed and forecast by the Norwegian mesoscale model system. The system is run operationally 4 times a day and provides high spatial and temporal resolution data for diagnostics in addition to daily forecasts. Both lows start developing as upper level vorticity maxima approach low-level baroclinic zones. One of the lows decays after the initial baroclinic intensification phase, while the other develops further. This second phase, the maintenance phase, seems to be related to organized convection. The possibility for air–sea interaction instability is discussed. The role of the underlying surface in creating conditions favourable for polar low developments is addressed as is the predictability of these mesoscale cyclones.

1. Introduction

The developing mechanism of polar lows is not fully understood. The problem was first addressed by Harley (1960) and Harrold and Browning (1969), who suggested that they are caused by baroclinic effects. Undoubtedly, baroclinic effects play a major role for the development of some (may be all) polar lows. Reed and Duncan (1987) showed a case study of a family of polar lows developing in a baroclinic reversed shear flow (the low advances in the opposite direction to the thermal wind). Quasi-geostrophic linear normal mode theory applied to the observed baroclinic fields gives growth rates and wave lengths comparable to observations. Recently, Peltier et al. (1990) used a primitive equation instability theory on the same data and obtained excellent results for growth rate, phase speed and wave length as compared to the analysis of Reed and Duncan (1987). In fact, by using the full primitive equations in normal mode baroclinic instability theory, a new instability mode is found. Peltier et al. (1990) speculate that this mode may be the mechanism working in polar lows, comma clouds and polar front cyclone disturbances.

The classical concept of a growing baroclinic disturbance from an infinitesimal perturbation has recently been challenged by Farell (1985, 1988) who instead views baroclinic developments as a finite-amplitude disturbance, i.e., an initial value problem. Farrell (1988) shows that the perturbation that results in the maximum growth of energy over a specified time interval may be found by solving a variational problem. In fact, the solution of this problem resembles an upper tropospheric trough approaching a surface centre as in the classical type-B cyclones (Pettersen et al., 1962).

A completely different theory for the growth and maintenance of polar lows is based on energy release through diabatic processes. In several papers (e.g., Rasmussen, 1981), Rasmussen has proposed that polar lows forming in the Atlantic Ocean are CISK driven. CISK (conditional instability of the second kind) is a self-exciting system where convection becomes sufficiently organized to have a positive feedback between the cloud scale and the developing vortex scale. Emanuel

(1986) has challenged the CISK concept arguing that in the atmosphere, there is little convective available energy present. Instead, he shows that tropical cyclones may be maintained entirely by interaction with the underlying warm sea. Emanuel and Rotunno (1989) have recently extended the theory to take sensible heat fluxes into account and have applied the theory on a polar low in the Norwegian Sea with good results.

It should be remarked that the air–sea interaction instability theory of Emanuel requires a finite disturbance precursor, e.g., a growing baroclinic wave. Several investigators (e.g., Reed, 1979; Sardie and Warner, 1983, 1985; Rasmussen, 1985) conclude that polar lows develop from a combination of baroclinic energy release and some kind of organized convection. There is no controversy about this conclusion since polar lows probably form under various atmospheric conditions as recognized by Lystad (1986) in his polar low classification. We still do not know, however, the relative importance of the various processes which trigger and maintain the growth of these lows.

Polar lows are frequently observed in the northern part of the Atlantic Ocean in the winter time (Rasmussen, 1983). The area is bounded by Norway, Spitsbergen, Greenland, Iceland and the British Isles. Typical for this area are large temperature contrasts at the surface due to a relatively warm sea, the ice-covered polar basin and the snow-covered land areas. Accordingly, there are always present a number of low-level baroclinic zones which may interact with upper-level disturbances.

In this paper, the developing and maintaining mechanism of polar lows will be addressed by a case study of two polar lows. From the large amount of lows developing each winter, we have chosen one from January 1987 and another from January 1988. The chosen lows are good candidates for the kind of processes we will demonstrate in this paper. They seem to be triggered by the same mechanism, but mature differently due to different environmental conditions. In order to compare the lows at different stages of development, we have chosen to jump from one case to the other. As a tool for the diagnostic analysis, we will use high-resolution data from the Norwegian mesoscale model system, which is run operational 4 times a day. The model system is described in Section 2 together with a synoptic review of the cases. In Section 3, we focus on the initial stages of the lows, relating them to theories about polar low development. Section 4 is dedicated to the mature phase of the lows while Section 5 contains a discussion of the role of the underlying surface and some speculations about the predictability of polar lows in the light of surface forcing. Section 6 provides a summary.

2. Numerical model and synoptic overview

While traditional diagnostic studies are based on data of temporal resolution 12 h (radiosondes), in principle one may extract data as often as one wishes from a numerical simulation. Combining observations and numerical products thus gives a data set with high temporal as well as spatial resolution for diagnostic studies. Recently, Uccellini et al. (1987) and Whitaker et al. (1988) used a numerical model to describe in detail the development and intensification of a case of strong cyclogenesis at the North American coast ("The President's Day Storm"). Keyser and Uccellini (1987) have reviewed the application of regional and mesoscale models to obtain high resolution and dynamically consistent data for diagnostic studies.

2.1. The model system

In this study, we will use the Norwegian mesoscale model system. The system, which contains procedures for data control, objective analysis, forecasting of weather elements, post-processing and diagnostics is briefly described in Table 1. The interested reader may find further details in the referenced papers. We will use a combination of objective analyses and forecasts of various lengths. The data are taken from the operational data assimilation/forecast cycle for one of the cases (January 1988), while the data for the other case (January 1987) is taken from a rerun where the model system was updated to the standard of Table 1. The polar low was forecast with the old version of the model system as well, but the new version gives slightly better results. The benefits and accuracy of using the data assimilation system for the January 1987 case are discussed in Midtbø et al. (1989).

Table 1. *The Norwegian mesoscale model system*

Pre-processing:	data control creation of data base data used: SYNOPS, SHIPS, AIREPS, BUOYS, TEMPS, PILOTS
Objective analysis:	(Bratseth, 1986; Grønås and Midtbø, 1987) optimum interpolation by successive corrections, first guess is 6-h mesoscale forecast
Forecast model:	(Grønås and Hellevik, 1982; Nordeng, 1986; Nordeng et al., 1988) explicit time integration (Bratseth, 1983) dynamic initialization (Bratseth, 1982) σ-coordinates, 10 levels $\Delta x = 50$ km, Arakawa D-grid surface layer fluxes (Louis et al., 1981) PBL fluxes (Blackadar, 1979) radiation/clouds (Nordeng, 1986) stratiform condensation (Nordeng, 1986) cloud liquid water convection (Geleyn, 1985)
Lateral boundaries:	forecasts from 150 km resolution LAM
SST and ice-edge:	climatological for the actual month
Post-processing:	all variables in p and σ-surfaces every 6 h stability profile interpolation within surface layer (Geleyn, 1988)
Diagnostics:	full interactive colour-plot system for model variables and derived variables horizontal and vertical sections, meteograms and soundings

A few comments should be made on the horizontal resolution. The method which is used for staggering and time integration (Bratseth, 1983) yields the same resolution for *all* horizontal derivatives of the governing equations. To obtain the same accuracy for the advection terms in the Arakawa C-grid, the resolution must be $\sqrt{2}$ times smaller (i.e., 35 km). The time integration method has an implicit horizontal diffusion which mainly affects wave lengths less than $3\Delta x$. There is no explicit horizontal diffusion.

2.2. *Synoptic overview*

At 0000 GMT 23 January 1987, a high-pressure system dominates the Atlantic Ocean so that the main baroclinic zone is found between 60° and 70°N. North of this area there are calm conditions and the air adjusts to the local forcing. Fig. 1 shows surface analysis from 1200 GMT 23 January 1987. At the east coast of Greenland, the temperature is -24°C while it varies from -15° to -20°C in the Svalbard area. In between, over relatively warm water, much higher temperatures are observed. A ship at (73°N, 2°E) reports of -1°C. One day later, a low starts to develop in the synoptic scale flow. The low is elongated in a northerly direction with a secondary low pressure centre west of Spitsbergen. The main low intensifies rapidly and crosses the Scandinavian peninsula during the next 24 h while the secondary low remains as a trough (Fig. 2). The 87-low develops in this trough during the night between 25 and 26 January. The satellite picture (Fig. 3) shows the low at 0830 GMT 26 January 1987.

One year later, a polar low developed close to Jan Mayen (73°55′N, 8°40′W). The low can hardly be detected on routine weather maps. Magnus Naustvig (personal communication) has identified several very small-scale lows forming at the east coast of Greenland prior to the low studied here. These lows were not described by the model system probably due to resolution. Fig. 4 shows the synoptic situation at 1200 GMT 25 January 1988. At this time, a small-scale upper level trough crosses Greenland (not shown). The low develops close to Jan Mayen 12 h later. The satellite picture from 0945 GMT 26 January 1988 (Fig. 5) shows the low with indications of warm and cold fronts in the middle of the Norwegian Sea. The analysis will show that the cold air outbreak in connection with the low east of Spitsbergen (Fig. 4) contributes to the development of the polar low.

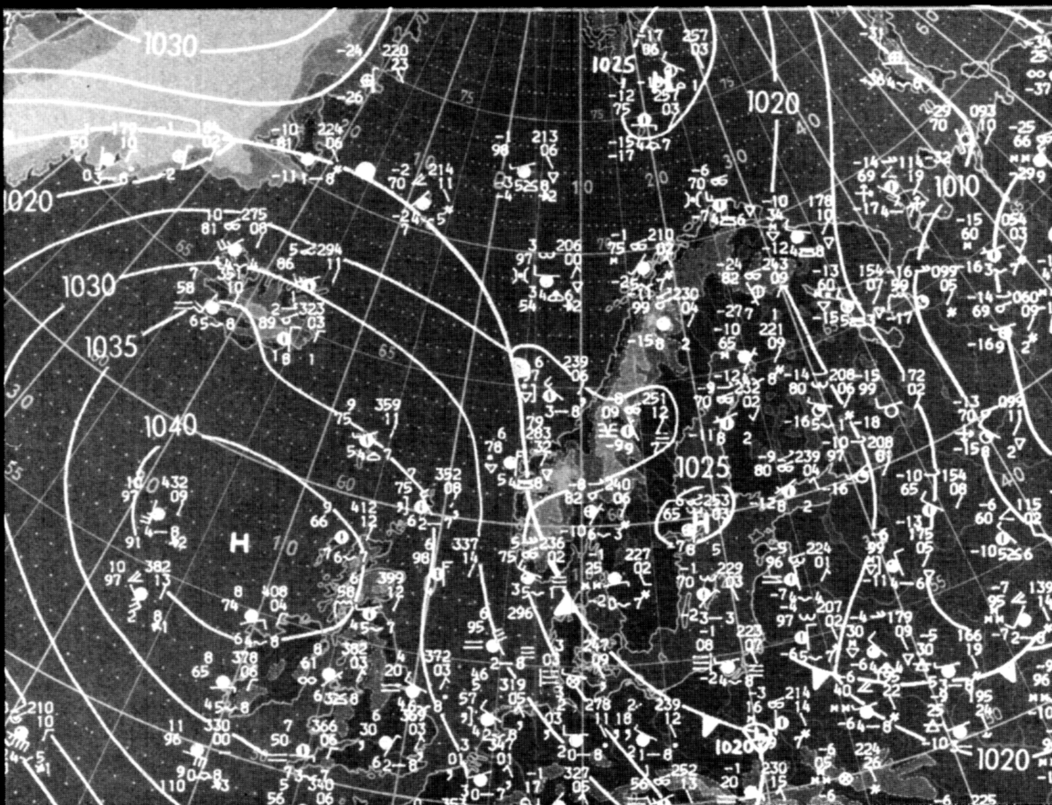

Fig. 1. Surface analysis for northern Europe for 1200 GMT 23 January 1987. (Europäische Wetterbericht)

3. The development phase

3.1. The low of January 1987

As explained in Section 2, a wedge of warm air and a low-level trough extending from the coast of Norway to 80° N along 10° E were present for several days prior to the development of the polar low of 26 January 1987. The role of the sea surface temperature anomaly in creating such a feature will be discussed in Section 5. The low developed between 1800 GMT 25 January 1987 and 0000 GMT 26 January 1987.

Fig. 6 shows the initial analysis and the 12- and 24-h forecasts from 0000 GMT 25 January 1987 together with the analysis at 0000 GMT 26 January 1987 of mean sea level pressure and 500 hPa heights. We notice that the model forecasts the development of the low as an upper level vorticity maximum detectable as a weak trough at 500 hPa (heavy stippled line in Fig. 6b) approaches from the polar basin. It should be mentioned that the trough shows up a bit more clearly at 700 hPa (not shown). In order to study the role of baroclinic versus diabatic processes, we have chosen to show vorticity advection with the thermal wind. It is well-known that there are large cancellations between the two main forcing terms of the quasi-geostrophic omega equation (differential vorticity advection and differential thickness advection) and that they may be simplified to vorticity advection with the thermal wind. Hoskins et al. (1978) have shown that they may be written in an even more compact form as the divergence of a vector. For the sake of simplicity and qualitative discussions, we will here use the vorticity advection by the thermal

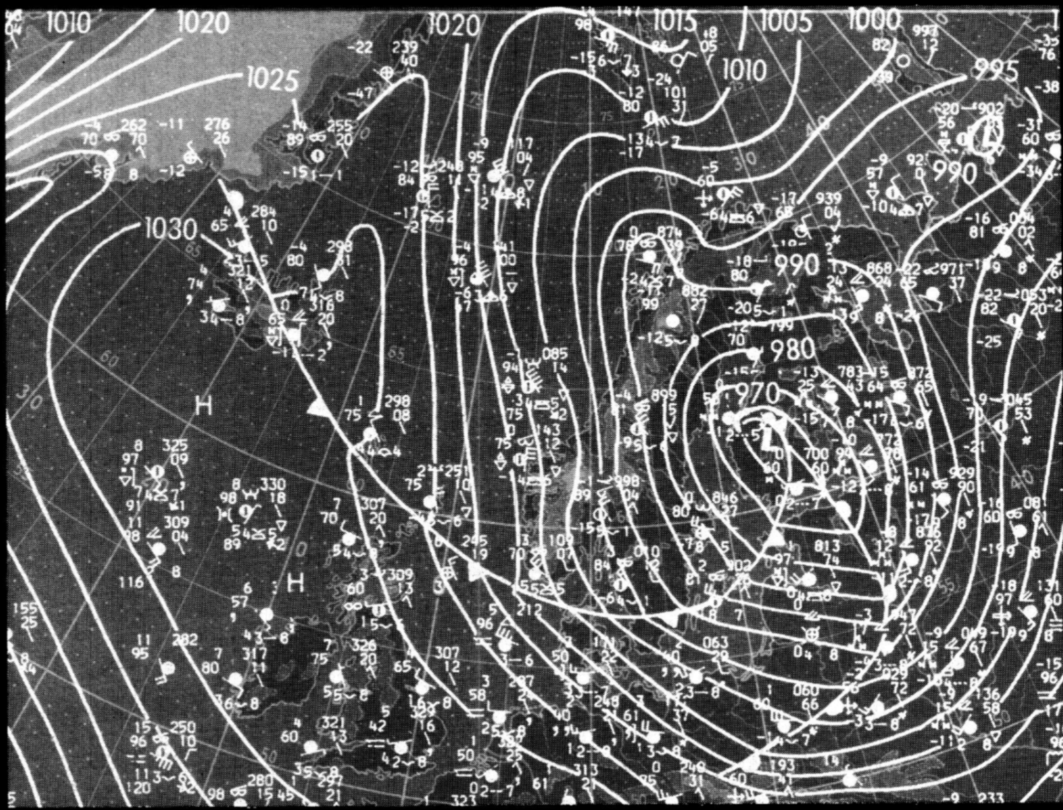

Fig. 2. Surface analysis for northern Europe for 1200 GMT 25 January 1987. (Europäische Wetterbericht)

wind. We should, however, be aware that we lose information about ω-forcing due to deformation and also by the ageostrophic motion, which may be important for strongly curved flow. The simplified omega-equation is,

$$\nabla^2 S\omega + f^2 \frac{\partial^2 \omega}{\partial p^2} = f \frac{\partial \mathbf{v}}{\partial p} \cdot \nabla(f + \zeta) - \nabla^2 H, \qquad (1)$$

where H is the contribution from diabatic effects and ζ is relative vorticity; S is static stability.

Fig. 7 shows contours of the mean temperature in the layer between 700 and 925 hPa together with relative vorticity at 850 hPa. The thermal wind ($\partial v/\partial z$) is parallel to the temperature contours with the coldest air to the left. From (1), one would expect ascending motion ($\omega < 0$) in regions where the right-hand side is positive. We therefore have the following qualitative result: ascending motion is found in regions where the thermal wind blows from high to low vorticity. The strength of the ω-forcing depends on the areal density of intersections between contours of temperature and vorticity, i.e., inversely proportional to the size of the solenoids formed by the intersections of adjacent pairs of temperature and vorticity. In regions of strong vertical velocity, one would expect vortex stretching and intensification. From Fig. 7a, we see that there is strong ω-forcing due to vorticity advection with the thermal wind in the initial stage of the development. Only 6 h later, however, this forcing is missing (Fig. 7b). Table 2 shows the life cycle of the low from 0600 GMT 25 January 1987 to 1800 GMT 26 January 1987. The last column is computed as the number of intersection points between contours of mean temperature between

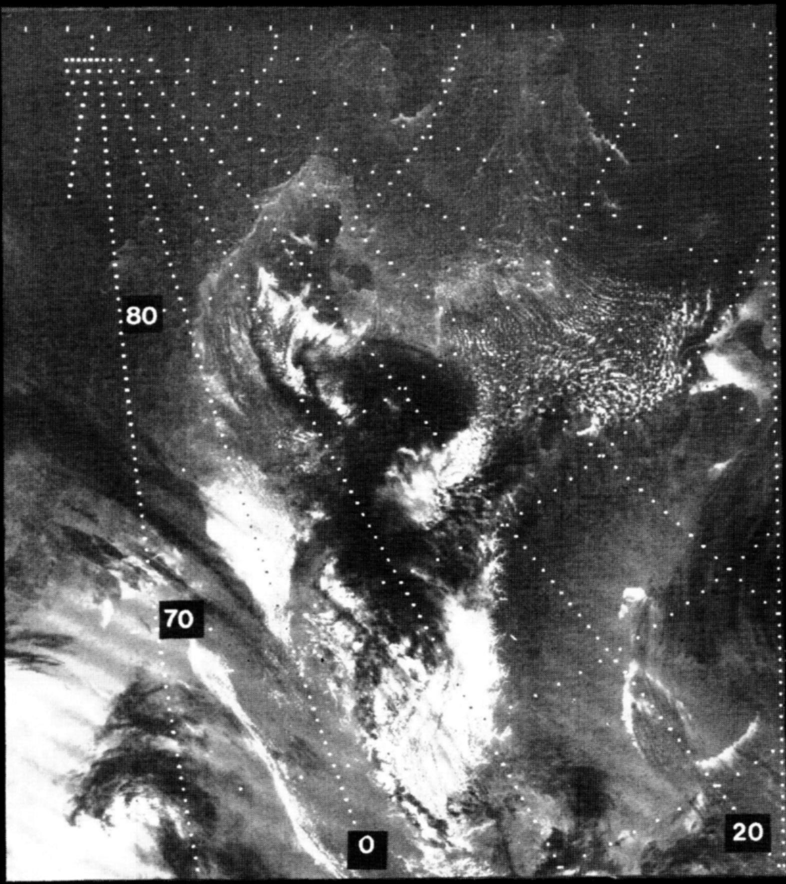

Fig. 3. Satellite picture (NOAA 10, infrared) valid at 0830 GMT 26 January 1987.

Table 2. *The life cycle of the low of 1987*

Verification time day/h	Sea level pressure analysis (hPa)	Sea level pressure 6 h-prognosis (hPa)	Maximum omega (hPa/s · 10^2)	Surface vorticity ($s^{-1} \cdot 10^4$)	Omega-forcing
25/0600	—	—	−1.0	—	—
25/1200	—	—	−1.4	2.0	12/4 ~3
25/1800	1005	1006	−1.8	3.5	14/6 ~2.5
26/0000	1003	1003	−2.2	4.5	26/13 ~2
26/0600	995	999	−1.2	3.5	3/3 ~1
26/1200	(997)	994	−1.6	3.0	5/9 ~0.5
26/1800	990	993	−1.0	2.0	—

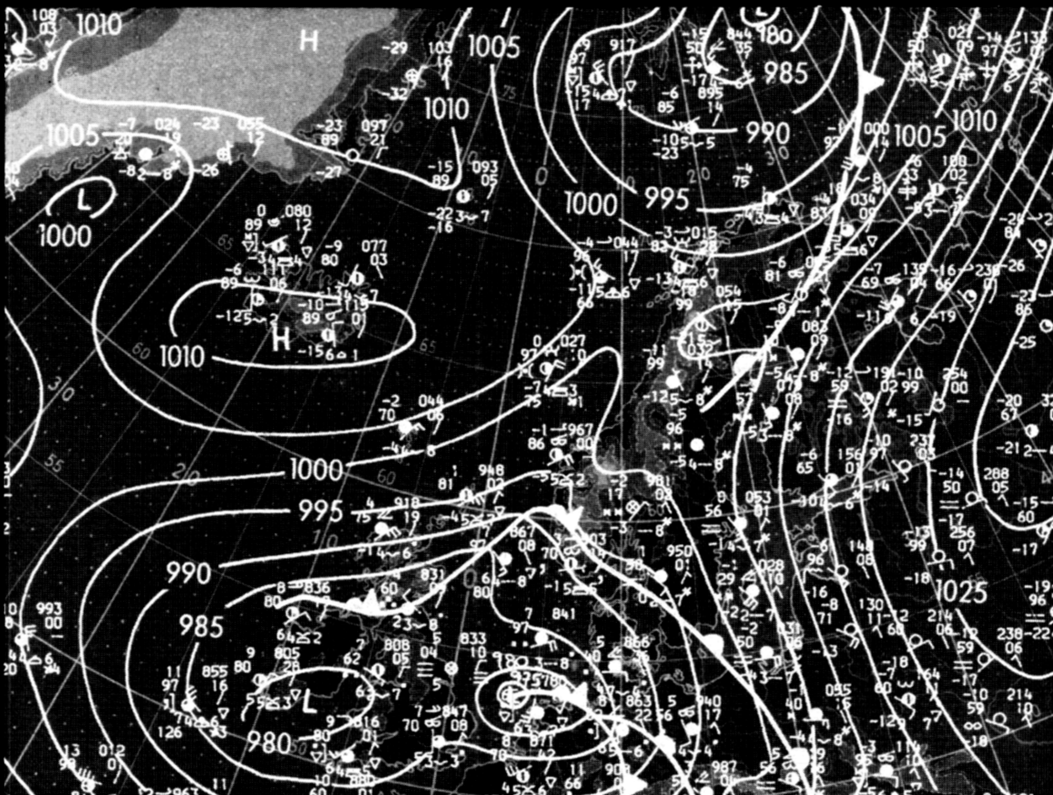

Fig. 4. Surface analysis for northern Europe for 1200 GMT 25 January 1988. (Europäische Wetterbericht)

700 and 1000 hPa and relative vorticity at 850 hPa within the area of strongest upward vertical velocity ($\omega < -1 \cdot 10^{-2}$ hPa/s) divided by the number of grid points in the same area. It measures the strength of the adiabatic forcing term of the quasi-geostrophic omega equation. The figures are taken from 6-h forecasts.

It is clearly seen that this forcing is largest during the initial phase of the development, indicating that the finite amplitude initial value theory of Farrell (1985) is important.

3.2. *The low of January 1988*

From contours of 700 hPa geopotential heights and mean sea level pressure, the polar low of 26 January 1988 resembles a common baroclinic development (Fig. 8). We shall see, however, that the low starts to deepen from a combination of events. First of all, the low forms close to the ice-edge. The low-level flow prior to and during the intensification phase is shown in Fig. 9. At 1800 GMT 25 January 1988, there is a strong baroclinic zone in connection with the ice-edge north of Iceland, shown as tight contours of equivalent potential temperature in Fig. 9a. Along this ice-bounded front, there is a low-level jet advecting warm air northwards. The jet is associated with a weak high and is nearly geostrophic. South of 70° N, there is strong shearing deformation, while a cold air outbreak is dominant in the northern part of the domain. The ageostrophic transverse frontal circulation (Fig. 10a), taken along cross-section AA′ in Fig. 9, is consistent with the forcing as described by the Eliassen–Sawyer equation (Eliassen, 1962). We notice that the circulation is shallow and that

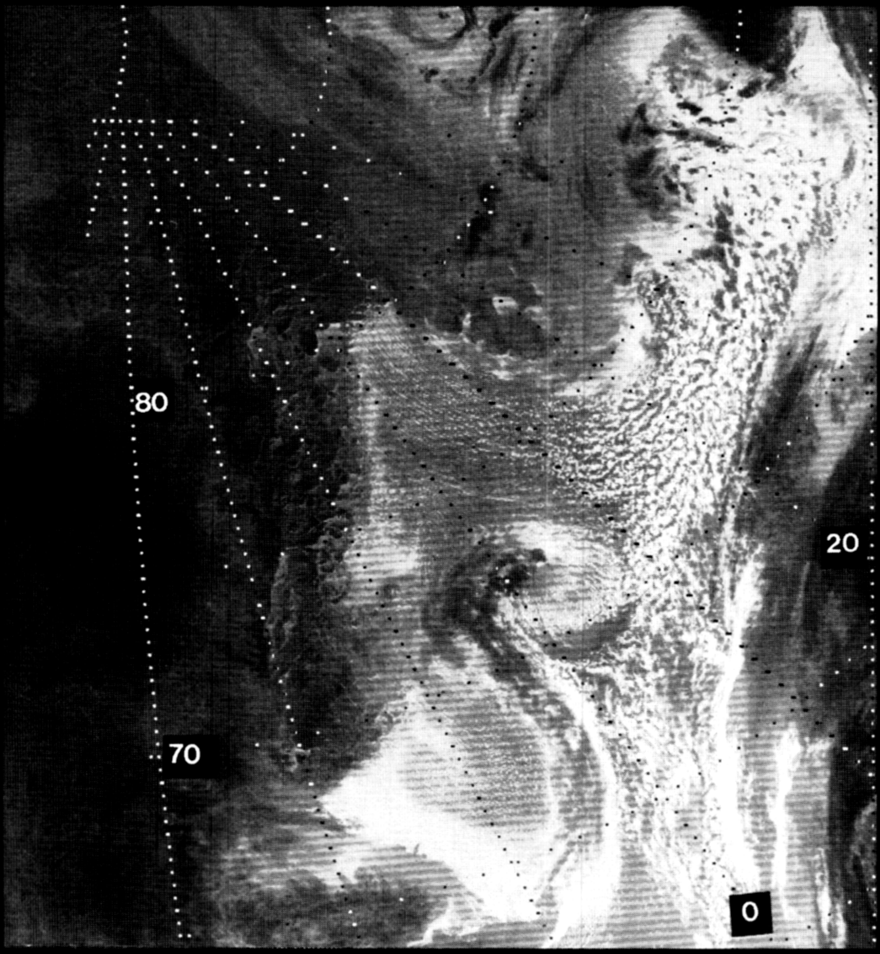

Fig. 5. Satellite picture (NOAA 10, infrared) valid at 0945 GMT 26 January 1988.

there is strong frontogenesis at low levels (Fig. 10a). 6 h later at 0000 GMT 26 January 1988, the circulation is stronger and deeper (Fig. 10b), the jet has brought warm, moist air further north and a strong cyclonic circulation has formed (Fig. 9b). As for the 87-low (Subsection 3.1), the intensification may be explained by traditional quasi-geostrophic theory. There is strong vorticity advection with the thermal wind around 700 hPa (Fig. 11) explaining the deeper and stronger circulation. Hence, there is vorticity creation from vortex stretching. In the early stages of the development, a cold air outbreak dominates the northern part of the domain (Fig. 9). Due to the induced cyclonic circulation from the approaching upper-level vorticity maximum, confluent deformation is created north of the circulation centre with strong frontogenesis. From this time, 0000 GMT 26 January 1988, the low intensifies rapidly and the strongest vertical velocity is actually found in connection with this newly formed front. A cross section (Fig. 12), along BB′ in Fig. 9c, shows the strong circulation around the cyclone centre, but also that the warm jet is elevated due to upgliding along the front and a contribution from the ageostorphic circulation. Note that the vertical velocity which is used to plot Figs. 10 and 12 is taken from the model run,

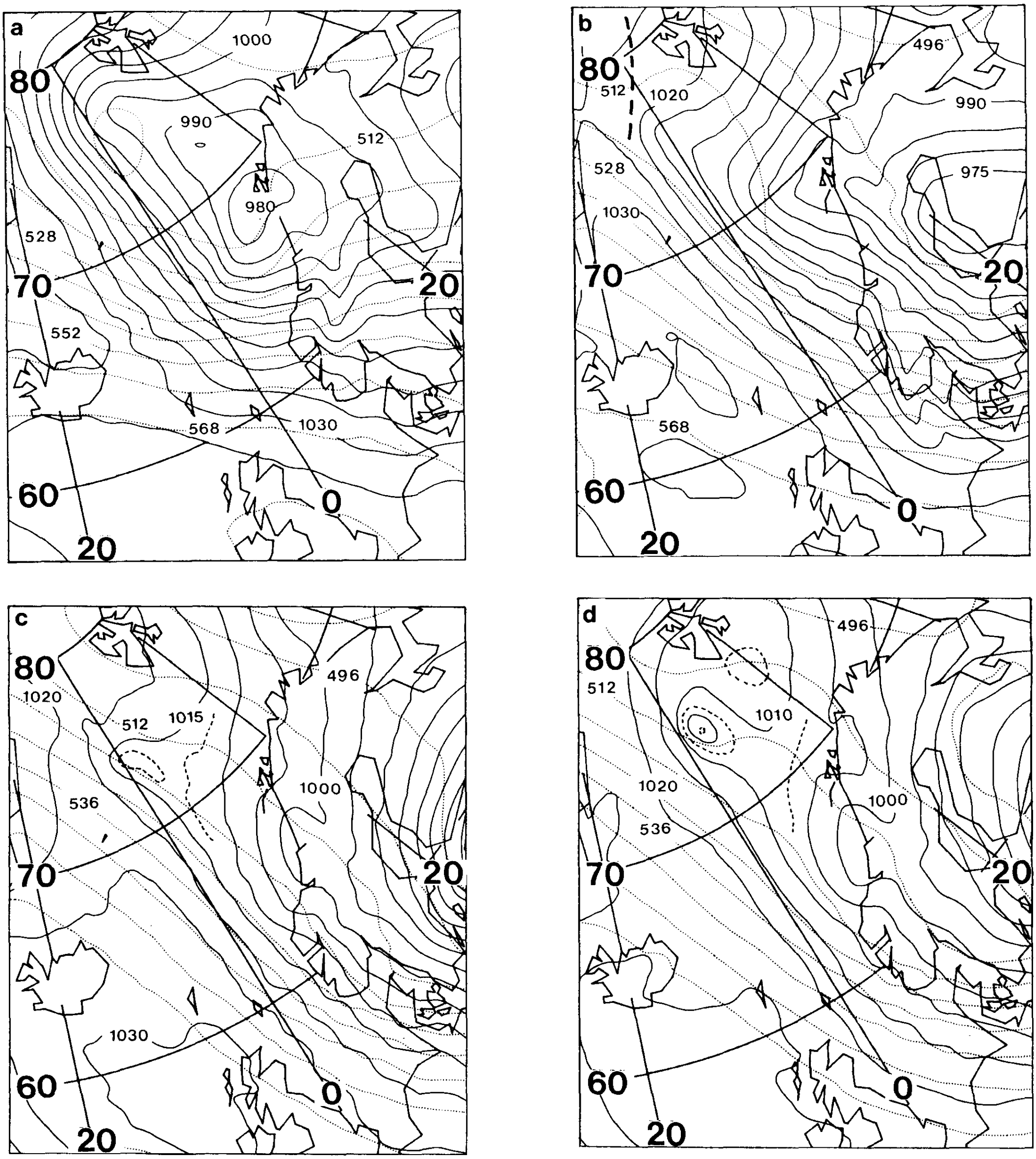

Fig. 6. Mean sea level pressure at contour intervals of 5 hPa (solid lines) and 500 hPa heights at intervals of 8 dam (dotted lines). (a) Initialized analysis of 0000 GMT 25 January 1987. (b) 12-h forecast valid at 1200 GMT 25 January 1987. (c) 24-h forecast valid at 0000 GMT 26 January 1987. Stippled lines signify 1012.5 hPa. (d) Initialized analysis 0000 GMT 26 January 1987. Stippled lines signify 1012.5, 1007.5 and 1002.5 hPa (the centre of the low).

while the ageostrophic wind is computed as the ageostrophic wind in the cross-section plane. The circulation is therefore somewhat misleading when the real ageostrophic motion is not confined to the chosen cross-section. The jet brings warm and moist air into the centre of the low, destabilizing the model atmosphere. Uccellini and Johnson (1979) showed an example where a

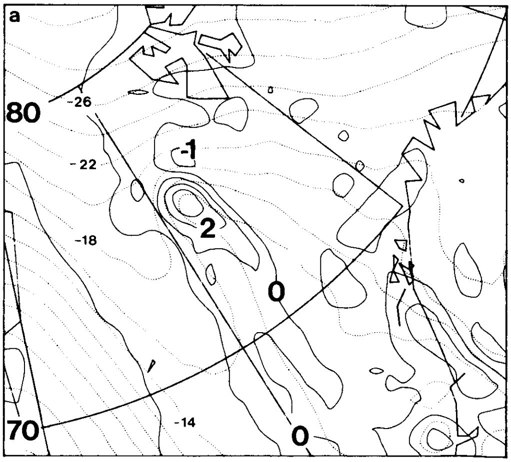

Fig. 7. 850 hPa relative vorticity at contour intervals of 10^{-4} s^{-1} (solid lines) and mean temperature in the layer between 700 and 925 hPa at contour intervals of 2 K (dotted lines). (a) 6-h forecast from 1800 GMT 25 January 1987; (b) 6-h forecast from 0000 GMT 26 January 1987.

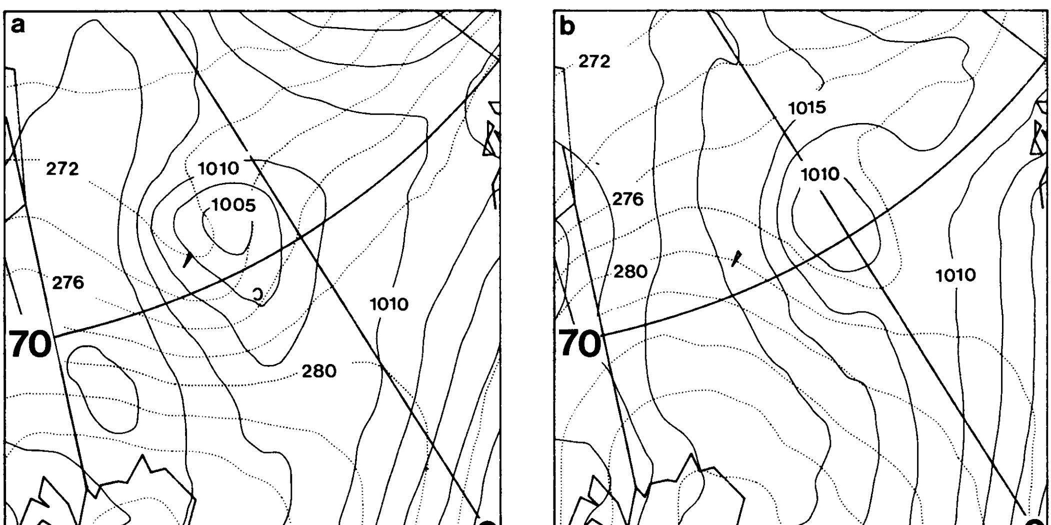

Fig. 8. Forecast from 0000 GMT 26 January 1988 of mean sea level pressure at contour intervals of 2.5 hPa (solid lines) and geopotential height of 700 hPa at intervals of 2 dam. (a) 6-h forecast; (b) 18-h forecast.

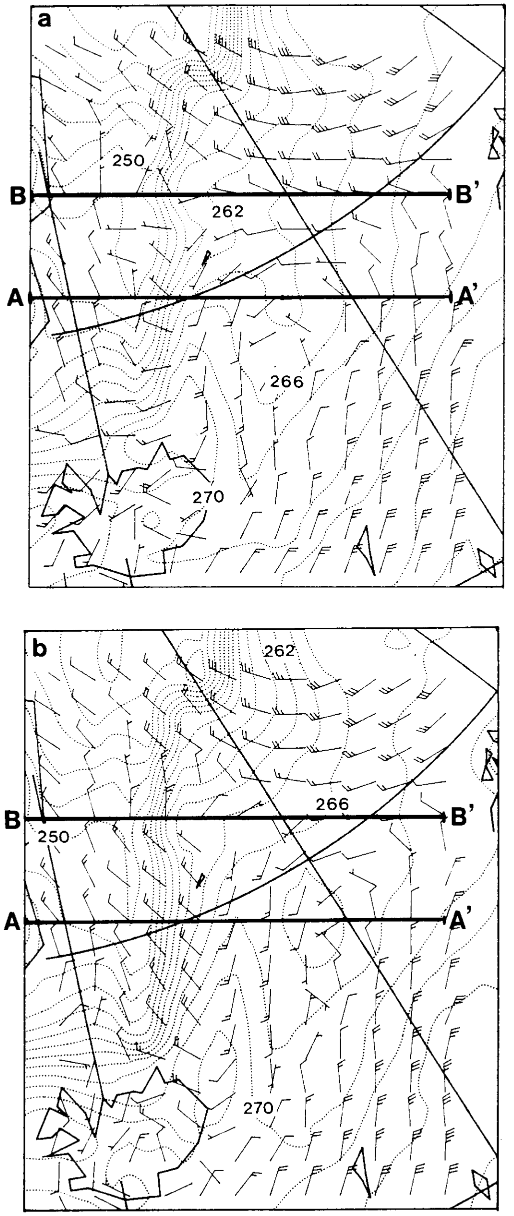

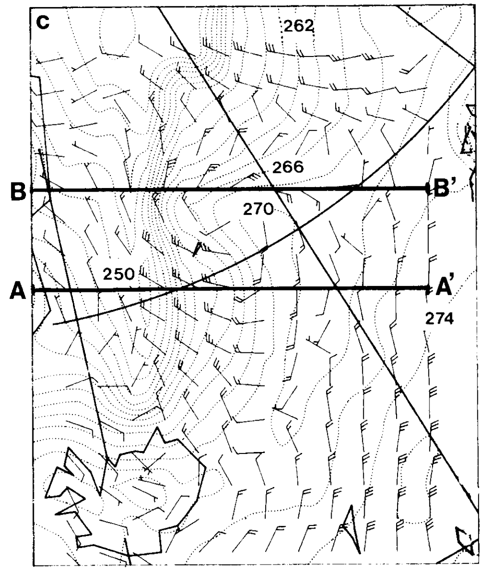

Fig. 9. Potential temperature in lowest model layer (≈ 40 m above surface) at contour intervals of 2 K (dotted lines) and winds in lowest model layer (every 2nd gridpoint plotted). Full barb = 5 m/s, half barb = 2.5 m/s. (a) 6-h forecast from 1200 GMT 25 January 1988; (b) 6-h forecast from 1800 GMT 25 January 1988; (c) 6-h forecast from 0000 GMT 26 January 1988. Heavy lines are cross-sections for Fig. 10 (AA′) and Fig. 12 (BB′).

low-level jet brings moist warm air and initiates a severe convective system. For the present case, a considerable amount of the predicted precipitation comes from the convective parameterization of the model.

For this case as well as the first case, the initial development phase is clearly described by baroclinic theory. For both cases, the lows intensify as upper level vorticity maxima approach low-level baroclinic zones, as in the B-type cyclones of Pettersen et al. (1962).

4. The maintenance and mature phases

4.1. The low of January 1987

From Table 1, we notice that the magnitude of the omega-forcing term decreases with time while the vertical velocity remains strong, indicating the differential heating gradually takes over as the main forcing term. It should be stressed that this partition is not unique. In curved flow, the geostrophic wind deviates significantly from the rotational wind so that the ageostrophic wind may have a rotational component. It should also be mentioned that diabatic effects may eventually alter the flow, giving rise to adiabatic forcing.

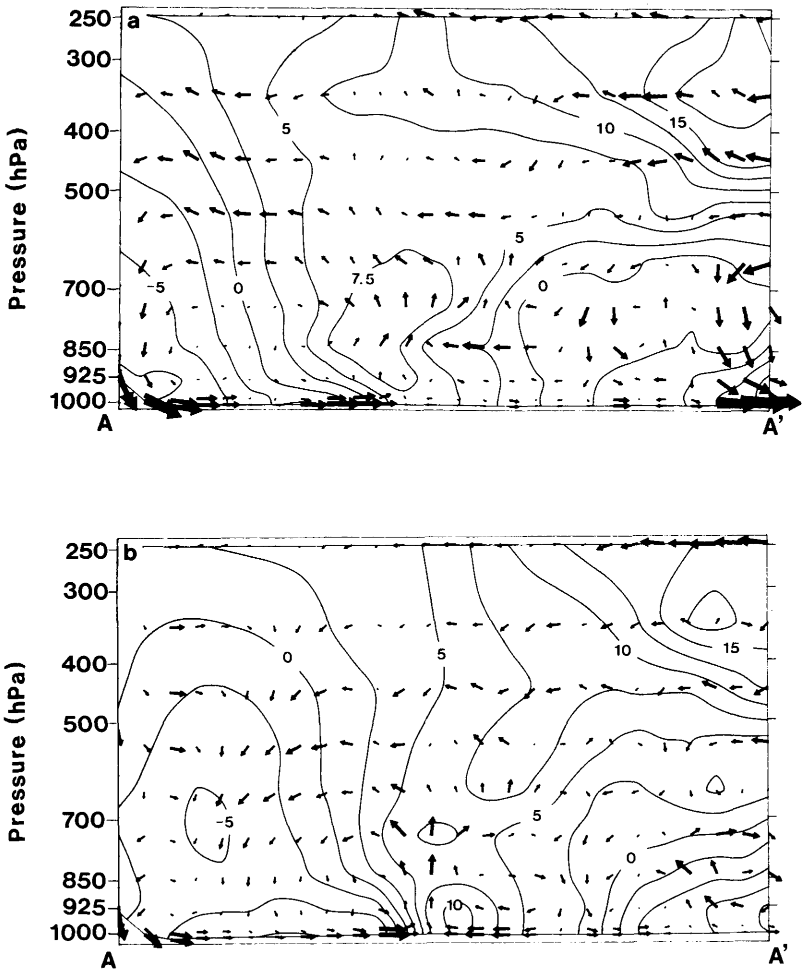

Fig. 10. Cross-section AA′ (Fig. 9) showing normal wind component, positive into paper, at contour intervals of 2.5 m/s and ageostrophic circulation in the x–p plane. The length of the arrows corresponds to a 3-h trajectory for a fixed wind speed and direction. The horizontal distance between the starting point of each arrow is 50 km. (a) 6-h forecast from 1200 GMT 25 January 1988; (b) 6-h forecast from 1800 GMT 25 January 1988.

The maximum vorticity decreases while the low deepens, showing that the scale of the low increases. During the fastest growth ($dp_s/dt \approx -1$ hPa/h), we find strong precipitation (≈ 1 mm/h). From the precipitation rate and the temperature difference between 500 hPa and the surface, we have estimated latent heating and adiabatic cooling from vertical advection of temperature. We find that these terms are approximately balanced, which is consistent with the conservative property of moist entrophy.

The possiblity for air–sea interaction instability (Emanuel, 1986; Emanuel and Rotunno, 1989) has been investigated. The theory views this kind of a cyclone as a Carnot engine so that heat acquired by surface fluxes balances frictional dissipation in the boundary layer and in the outflow. In the steady state limit, the theory

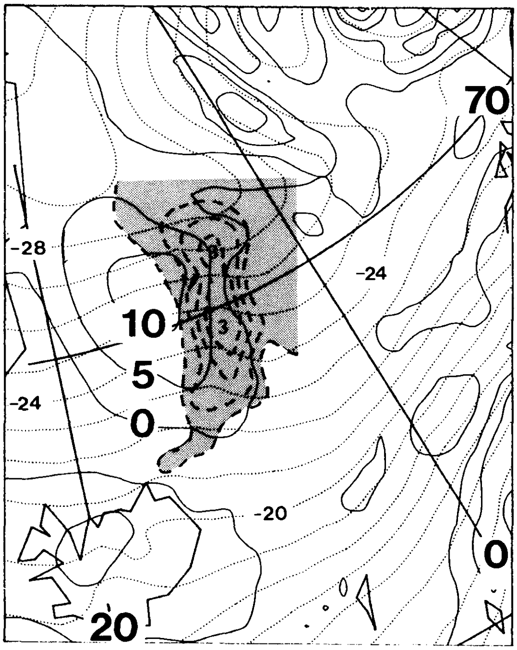

Fig. 11. 700 hPa relative vorticity at contour intervals of $5 \cdot 10^{-5}\ \mathrm{s}^{-1}$ (solid lines), mean temperature in the layer between 500 and 925 hPa at contour intervals of 1 K (dotted lines) and some contours of vertical velocity at model level 6 (≈ 650 hPa) at intervals of 10^{-3} hPa/s (dashed lines). Ascending area in connection with the vorticity maximum (see text) is shaded. Valid at 0000 GMT 26 January 1988.

predicts the central pressure for a cyclone maintained entirely by surface fluxes. The central pressure may be estimated from (Emanuel and Rotunno, 1989),

$$x = \exp(-a/x - b), \tag{2}$$

where $x = p_c/p_a$ is the ratio of central pressure to ambient pressure, and

$$a = \frac{e_c}{p_a}\left(\frac{\varepsilon}{1-\varepsilon}\frac{L_v}{R_v T_c}\right), \tag{4}$$

$$b = \frac{T_c - T_a}{T_c}\left(\frac{\varepsilon}{1-\varepsilon}\frac{c_p}{R}\right) - \frac{e_a}{p_a}\left(\frac{\varepsilon}{1-\varepsilon}\frac{L_v}{R_v T_c}\right). \tag{5}$$

Taking $e_c = 6.11$ hPa, $p_a = 1005$ hPa, $T_c = 273$ K, $T_a = 268$ K, $e_a = 4.21$ hPa and $T_{out} = 238$ K, we get the thermodynamic efficiency,

$$\varepsilon = (T_c - T_{out})/T_c = 0.128,$$

and $p_c = 990$ hPa. These numbers are taken from a 6-h forecast from 0000 GMT 26 January. The forecast surface pressure at this time is 994 hPa and drops to 990 hPa 6 h later.

Strictly speaking, the theory is valid for axisymmetric cyclones only. The low studied here does not satisfy this criterion. It is particularly difficult to find a unique outflow temperature. We have defined the outflow temperature T_{out} as the mean temperature at levels of maximum divergence (i.e., outflow) around the low. (In subsidence areas, this means surface tempera-

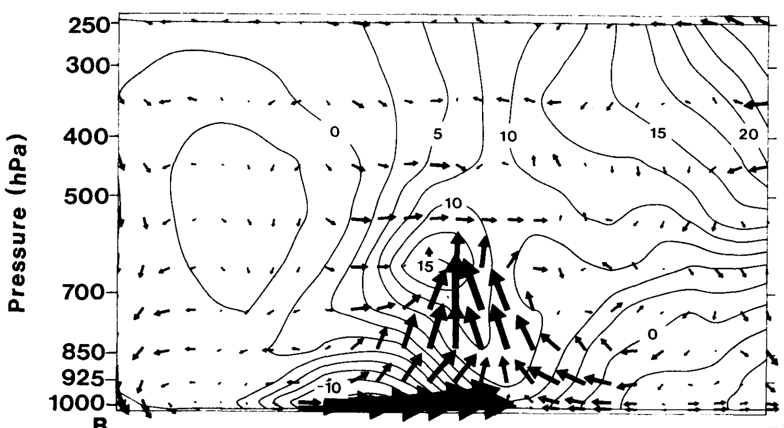

Fig. 12. Same as Fig. 10, but cross-section BB′ in Fig. 9 and 6-h forecast from 0000 GMT 26 January 1988.

ture). Air–sea interaction instability theory requires a finite amplitude precursor. If the theory is applicable to this low, baroclinic instability release from the approaching upper level wave seems to play the role of a precursor.

The low rapidly dissipates after making landfall, supporting the air–sea interaction instability theory, or at least showing that the warm sea is a necessary condition for the maintenance of the low.

4.2. The low of January 1988

This low shows no signs of a further growth after the initial baroclinic development phase. It reaches maximum intensity at 0600 GMT 26 January 1988 (Fig. 8a). 12 h later, the sea level pressure low and the upper level trough are in phase (Fig. 8b), and from now on, the low quickly dissipates as it becomes suppressed by a synoptic scale flow regime.

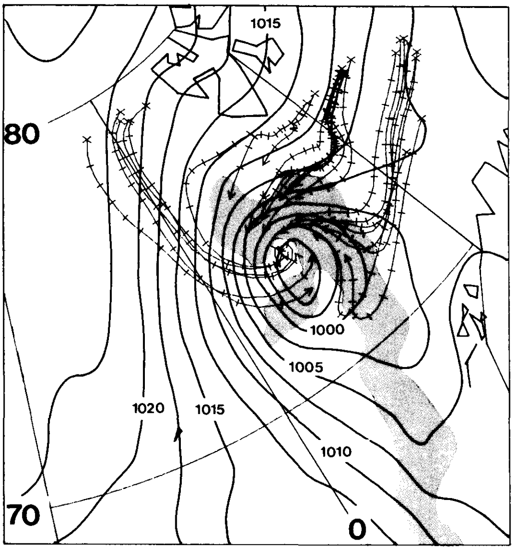

Fig. 13. Mean sea level pressure at contour intervals of 2.5 hPa (solid lines) and 24-h surface wind trajectories ending at 1200 GMT 26 January 1987, based on initialized analyses and short-range forecast winds (+2 and +4 h) from the lowest model layer (≈ 40 m) with temporal resolution 2 h. Shaded area signifies 2-h accumulated precipitation at the end of the period.

5. The role of the underlying surface

5.1. The low of January 1987

Fig. 13 shows surface air trajectories ending in the vicinity of the low at 1200 GMT 26 January 1987 and surface pressure. The area of predicted precipitation (accumulated in 2 h) is shaded. The trajectories are divided into 3 main groups. The northern group ends close to the centre of the low where there is mainly subsidence. The 2 other groups come from the east and feed the updraughts. The southernmost of these passes a long distance over the open sea, while the other passes over the ice a part of the time. At 1200 GMT 25 January 1987, the equivalent potential temperature at the starting point of the southern group of trajectories is approximately 260 K. One day later, when the same air enters the inner regions of the cyclone, the equivalent potential temperature is 280 K, showing a "heating" rate close to 1 K/h. A necessary condition for the air–sea interaction instability theory of Emanuel (1986) is that air parcels acquire heat from the underlying surface as they spiral towards the cyclone centre.

This study indicates that the low formed as an upper level trough approached a low-level vorticity maximum created by a trough of warm air west of Spitzbergen. A similar tongue of warm air was found in several of the cases studied numerically by Grønås et al. (1987) and in one of the cases studied by Nordeng (1987) and is probably connected to a branch of the Gulf Stream which heads northwards along the western coast of Spitzbergen. The warm sea creates a wedge-shaped ice-free region which extends almost to 80° N all year round. The air is heated from the underlying warm sea. Consistent with this, there is surface pressure drop and vorticity creation. In addition to this process, which makes the area sensitive to baroclinic developments, the relatively warm water is favourable for initiation of convection. We believe that this may explain why there is a maximum of polar low developments in this area, as shown by Lystad (1986).

5.2. The low of January 1988

The importance of a correct description of the underlying surface is also demonstrated for this low. The low intensifies as an upper-level wave crosses Greenland and interacts with a low-level baroclinic zone created by the fixed ice-edge ("fixed" means relative to the time-scale of the atmospheric disturbances). The low develops its own fronts, seen as gradients of equivalent potential temperature in Fig. 14, while the ice-edge bound front regenerates. The fronts in Fig. 14 are drawn subjectively from the equivalent potential temperature contours.

The low dissipates quickly after the baroclinic phase. One reason may be an approaching polar front cyclone suppressing further development. The low has, however, no potential for growth beyond the intensity of 0600 GMT 26 January 1988 as described by the air–sea interaction theory. Introducing appropriate numbers for T_{out}, T_c, p_a etc.) from 0600 GMT 26 January 1988 into eqs. 2–5 ($T_c = 269$ K, $T_{out} = 242$ K, $T_a = 267$ K, $p_a = 1010$ hPa) gives $p_c = 1003.6$ hPa. The surface trajectories (in Fig. 15) ending up in the area of strongest updraught (those from the north) have mainly passed the ice-covered sea and have picked up very little energy from the underlying surface.

5.3. *Predictability*

This study has some relevance for the predictability of the mesoscales. In fact, both lows were forecast with the model system from more than one day ahead, and both lows develop as upper-level troughs interact with "stationary" low-level baroclinic zones. It is of course impossible to draw a general conclusion from two cases, but if this is a typical development pattern for polar lows, it means that the task of forecasting polar lows is possible. The forecasting problem is reduced to forecasting the upper level vorticity maxima correctly, since the low-level baroclinic zones are so strongly related to fixed surface features. Fortunately, the upper-level dis-

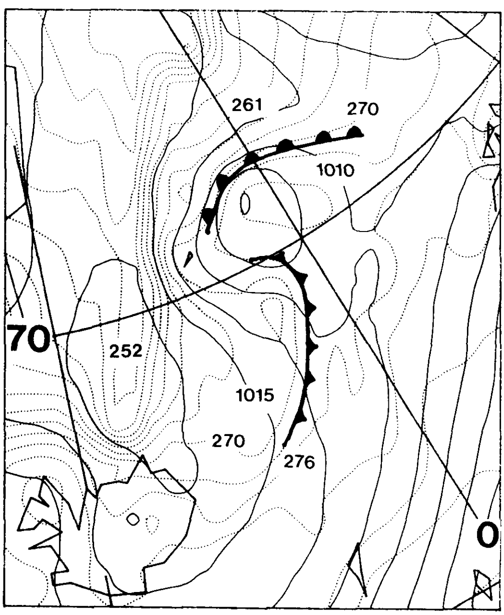

Fig. 14. Mean sea level pressure at contour intervals of 2.5 hPa (solid lines) and equivalent potential temperature from lowest model layer at contour intervals of 3 K (dotted lines). 12-h forecast from 0000 GMT 26 January 1988. The fronts are drawn subjectively from the θ_e lines.

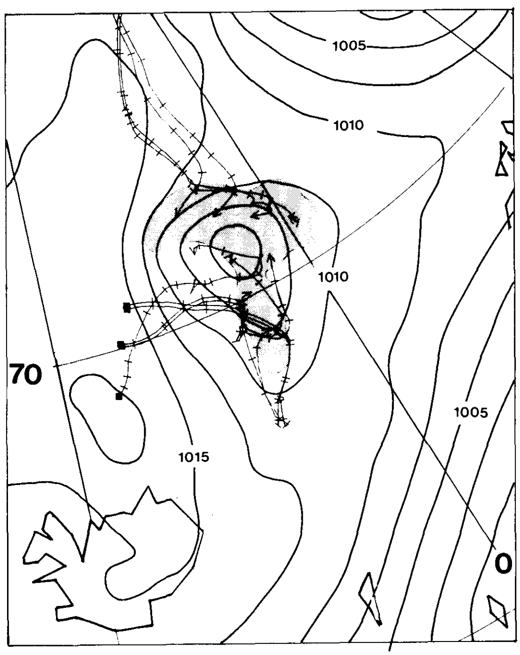

Fig. 15. Same as Fig. 13, but 30-h trajectories ending at 0600 GMT 26 January 1988 based on initialized analyses of winds of temporal resolution 6 h. Shaded area signifies 3-h accumulated precipitation at the end of the period.

turbances often have a larger scale than the polar lows and may therefore be recognized and analysed. With the present schemes for parameterization of convection, we may not be able to simulate the very intense hurricane-like phase (Nordeng et al., 1989), possibly driven by air–sea interaction instability, but we have at least a chance to forecast (and therefore detect) the initial baroclinic phase of the lows.

6. Summary

The development and maintenance mechanisms of polar lows have been addressed by case studies of two polar lows from the Norwegian Sea. The lows develop through a series of events, but the main triggering mechanism for both cases is approaching upper level troughs or vorticity maxima. The low-level baroclinic zones which interact with the upper-level disturbances are created by the "fixed" surface forcing, i.e., sea surface temperature anomaly and ice-edge.

The air–sea interaction theory of Emanuel (1986) and Emanuel and Rotunno (1989) describes how cyclones may be maintained and grow entirely through energy acquired from the sea. Applying this theory on the two lows studied here may explain why one of the lows continues to grow when there is no more potential energy to convert to kinetic energy by baroclinic processes. In addition, the theory correctly shows that there is no potential for further growth of the second low.

Finally, the predictability task for these mesoscale cyclones is discussed in the light of the results from this study, and we end up with the somewhat speculative conclusion that (some) polar lows seem to be predictable, because it is the action of a (predictable) upper-level forcing on a fixed-surface feature that triggers their development.

7. Acknowledgement

The author is obliged to Dr. Melvin A. Shapiro for fruitful discussions and helpful suggestions in analysing the dynamics of the lows.

REFERENCES

Blackadar, A. K. 1979. High resolution models of the planetary boundary layer. *Advances in environment and scientific engineering*. London: Gordon and Breach, 276 pp.

Bratseth, A. M. 1982. A simple and efficient approach to the initialization of weather prediction models. *Tellus 34*, 352–357.

Bratseth, A. M. 1983. Some economical, explicit finite-difference schemes for the primitive equations. *Mon. Wea. Rev. 111*, 663–668.

Bratseth, A. M. 1986. Statistical interpolation by means of successive corrections. *Tellus 38A*, 449–457.

Eliassen, A. 1962. On the vertical circulation in frontal zones. *Geophys. Norvegica 24*, 147–160.

Emanuel, K. A. 1986. An air–sea interaction theory for tropical cyclones. Part I: Steady-state maintenance. *J. Atmos. Sci. 43*, 585–604.

Emanuel, K. A. and Rotunno, R. 1989. Polar lows as arctic hurricanes. *Tellus 41A*, 1–17.

Farrell, B. 1985. Transient growth of damped baroclinic waves. *J. Atmos. Sci. 42*, 2718–2727.

Farrell, B. 1988. Cyclogenesis as an initial value problem: theory and implications. Preprint Palmén Memorial Volume, Amer. Met. Soc.

Geleyn, J.-F. 1985. On a simple parameter-free partition between moistening and precipitation in the Kuo scheme. *Mon. Wea. Rev. 113*, 405–407.

Geleyn, J.-F. 1988. Interpolation of wind, temperature and humidity from model levels to the height of measurements. *Tellus 40A*, 347–351.

Grønås, S. and Hellevik, O. E. 1982. A limited area prediction model at the Norwegian Meteorological Institute. *Techn. rep. No. 61*. Norwegian Meteorological Institute, Oslo, Norway.

Grønås, S. and Midtbø, K. H. 1987. Operational multivariate analyses by successive corrections. *Collection of papers presented at the WMO/IUGG NWP symposium Tokyo, 4–8 August 1986*. Meteorol. Soc. Japan.

Grønås, S., Foss, A. and Lystad, M. 1987. Numerical simulations of polar lows in the Norwegian Sea. *Tellus 39A*, 334–354.

Harley, D. G. 1960. Frontal contour analysis of a "polar" low. *Met. Mag. 89*, 141–147.

Harrold, T. W. and Brownig, K. A. 1969. The polar low as a baroclinic disturbance. *Q. J. R. Meteorol. Soc. 95*, 710–723.

Hoskins, B. J., Draghici, I. and Davies, H. C. 1978. A new look at the omega equation. *Q. J. R. Meteorol. Soc. 104*, 31–38.

Keyser, D. and Uccellini, L. W. 1987. Regional models: emerging research tools for synoptic meteorologists. *Bull. Amer. Meteor. Soc. 68*, 306–320.

Louis, J.-F., Tiedtke, M. and Geleyn, J.-F. 1981. *A short history of the operational PBL-parameterization at ECMWF. Workshop on planetary boundary layer parameterization*, European Centre for Medium Range Weather Forecasts, Shinfield Park, Reading, England.

Lystad, M. 1986. *Polar lows in the Norwegian, Greenland and Barents Sea. Final report of the Polar Lows Project.* The Norwegian Meteorological Institute, P.O. Box 43—Blindern, 0313 Oslo 3, Norway.

Midtbø. K. H., Grønås, S., Lystad, M. and Nordeng, T. E. 1989. Analyses of polar lows in the Norwegian Sea with a mesoscale limited area NWP system. In: *Polar/Arctic lows* (eds. Paul Twitchell, Erik Rasmussen and Ken Davidson). Virginia, USA: A. Deepak Publishing.

Nordeng, T. E. 1986. Parameterization of physical processes in three-dimensional numerical weather prediction model. *Techn. Rep. No. 65.* Norwegian Meteorological Institute, Oslo, Norway.

Nordeng, T. E. 1987. The effect of vertical and slantwise convection on the simulation of polar lows. *Tellus 39A*, 354–376.

Nordeng, T. E., Reistad, M. and Magnusson, A. K. 1988. An optimum use of atmospheric data in wind wave modelling—numerical experiments. *Techn. rep. No. 68.* Norwegian Meteorological Institute, Oslo, Norway.

Nordeng, T. E., Foss, A., Grønås, S., Lystad, M. and Midtbø, K. H. 1989. On the role of resolution and physical parameterization for numerical simulations of polar lows. In: *Polar/Arctic lows* (eds. Paul Twitchell, Erik Rasmussen and Ken Davidson). Virginia: USA: A. Deepak Publishing.

Peltier, W. R., Kent Moore, G. W. and Polavarapu, S. 1990. Cyclogenesis and frontogenesis. *Tellus 42A*, in press.

Pettersen, S., Bradbury, D. L. and Pedersen, K. 1962. The Norwegian cyclone models in relation to heat and cold sources. *Geophys. Norvegica 24*, 243–280.

Rasmussen, E. 1981. An investigation of a polar low with a spiral cloud structure. *J. Atmos. Sci. 38*, 1785–1792.

Rasmussen, E. 1983. A review of mesoscale disturbances in cold air masses. In: *Mesoscale meteorology—theories, observations and models* (eds. D. K. Lilly and T. Gal-chen). Boston: D. Reidel Publishing Company, 246–283.

Rasmussen, E. 1985. A case study of a polar low development over the Barents Sea. *Tellus 37A*, 407–418.

Reed, R. J. 1979. Cyclogenesis in polar air streams. *Mon. Wea. Rev. 107*, 38–52.

Reed, R. J. and Duncan, C. N. 1987. Baroclinic instability as a mechanism for the serial development of polar lows: a case study. *Tellus 39A*, 376–384.

Sardie, J. M. and Warner, T. T. 1983. On the mechanism for the development of polar lows. *J. Atmos. Sci. 40*, 869–881.

Sardie, J. M. and Warner, T. T. 1985. A numerical study of the development mechanism of polar lows. *Tellus 37A*, 460–477.

Uccellini, L. W. and Johnson, D. R. 1979. The coupling of upper- and lower-tropospheric jet streaks and implications for the development of severe convective storms. *Mon. Wea. Rev. 107*, 682–703.

Uccellini, L. W., Petersen, R. A., Brill, K. F., Kocin, P. J. and Tuccillo, J. J. 1987. Synergistic interactions between an upper-level jet streak and diabatic processes that influence the development of a low-level jet and a secondary coastal cyclone. *Mon. Wea. Rev. 115*, 2227–2261.

Whitaker, J. S., Uccellini, L. W. and Brill, K. F. 1988. A model-based diagnostic study of the rapid development phase of the Presidents' Day cyclone. *Mon. Wea. Rev. 116*, 2337–2365.